Journal of Cerebral Blood Flow & Metabolism (2010) 30, 1661–1670
© 2010 ISCBFM All rights reserved 0271-678X/10 $32.00
www.jcbfm.com

Artificial neural network prediction of ischemic tissue fate in acute stroke imaging

Shiliang Huang[1,6], Qiang Shen[1,2,6] and Timothy Q Duong[1,2,3,4,5]

[1]*Research Imaging Institute, UT Health Science, San Antonio, Texas, USA;* [2]*Department of Ophthalmology, UT Health Science, San Antonio, Texas, USA;* [3]*Department of Radiology, UT Health Science, San Antonio, Texas, USA;* [4]*Department of Physiology, UT Health Science, San Antonio, Texas, USA;* [5]*South Texas Veterans Health Care System, San Antonio, Texas, USA*

Multimodal magnetic resonance imaging of acute stroke provides predictive value that can be used to guide stroke therapy. A flexible artificial neural network (ANN) algorithm was developed and applied to predict ischemic tissue fate on three stroke groups: 30-, 60-minute, and permanent middle cerebral artery occlusion in rats. Cerebral blood flow (CBF), apparent diffusion coefficient (ADC), and spin–spin relaxation time constant (T2) were acquired during the acute phase up to 3 hours and again at 24 hours followed by histology. Infarct was predicted on a pixel-by-pixel basis using only acute (30-minute) stroke data. In addition, neighboring pixel information and infarction incidence were also incorporated into the ANN model to improve prediction accuracy. Receiver-operating characteristic analysis was used to quantify prediction accuracy. The major findings were the following: (1) CBF alone poorly predicted the final infarct across three experimental groups; (2) ADC alone adequately predicted the infarct; (3) CBF + ADC improved the prediction accuracy; (4) inclusion of neighboring pixel information and infarction incidence further improved the prediction accuracy; and (5) prediction was more accurate for permanent occlusion, followed by 60- and 30-minute occlusion. The ANN predictive model could thus provide a flexible and objective framework for clinicians to evaluate stroke treatment options on an individual patient basis.
Journal of Cerebral Blood Flow & Metabolism (2010) **30,** 1661–1670; doi:10.1038/jcbfm.2010.56; published online 28 April 2010

Keywords: ANN; DWI; ischemic penumbra; perfusion–diffusion mismatch; predictive model; PWI

Introduction

Multimodal magnetic resonance imaging (MRI) of acute stroke provides clinically relevant data and predictive value to guide stroke therapy. Combined perfusion- and diffusion-weighted MRI is remarkably sensitive in detecting acute stroke changes and is becoming the method of choice for diagnosis, staging, and characterization of ischemic brain injury. The anatomical mismatch between perfusion and diffusion abnormality (Kidwell *et al*, 2003; Warach, 2003) approximates the potentially salvageable 'ischemic penumbra' (Astrup *et al*, 1981*a*, *b*; Hossmann, 1994; Lo *et al*, 2005). Although the definition of perfusion–diffusion mismatch has evolved slightly over the years (Kidwell *et al*, 2003), it remains widely used to guide acute stroke treatment in emergency rooms. In contrast, conventional T2-weighted MRI could not detect ischemic injury until at least 6 hours after stroke onset, coinciding with vasogenic edema, at which point the tissue is likely already infarcted.

Prediction of infarct volume on a pixel-by-pixel basis has been demonstrated using critical thresholds of the apparent diffusion coefficient (ADC) or cerebral blood flow (CBF) values (Arenillas *et al*, 2002; Thomalla *et al*, 2003). Although this approach is simplistic and has limitations, it is practical for evaluating treatment effects on lesion volumes. A more sophisticated prediction algorithm used a voxel-based generalized linear model (GLM) to predict tissue infarction in middle cerebral artery occlusion (MCAO) in rats (Wu *et al*, 2007) and human stroke patients (Wu *et al*, 2001). Predicted outcome was compared with the tissue's histology or end-point T2 imaging. Shen *et al* (2005*b)* introduced another predictive model based on the probability of infarct (Shen and Duong, 2008). This model documented the probability-of-infarct profiles of stroke

Correspondence: Dr TQ Duong, Research Imaging Institute, UT Health Science San Antonio, 8403 Floyd Curl Drive, San Antonio, TX 78229, USA.
E-mail: duongt@uthscsa.edu
[6]These two authors contributed equally to this work.
This work was supported by the NIH (R01-NS45879) and the American Heart Association (SDG-0430020N and SDG-0830293N).
Received 31 August 2009; revised 23 February 2010; accepted 24 March 2010; published online 28 April 2010

rats that underwent different occlusion durations. Predictions, which were made based on acute stroke data in the form of probability-of-infarct maps, showed the likelihood of future infarction on a pixel-by-pixel basis. Performance analysis showed accurate prediction when compared with end-point T2 MRI and histology. These predictive algorithms have the potential to serve as promising metrics for diagnosis, prognosis, and therapeutic evaluation of acute stroke.

The evolution of ischemic injury is spatially heterogeneous (Guadagno *et al*, 2005; Sobesky *et al*, 2005). Although acute ADC and CBF data are very informative in predicting outcome, other factors could also affect stroke outcome. Two of these factors are neighboring pixel information and infarction incidence. First, a single pixel or a small island of normal pixels in the hyperacute phase is often surrounded by severe ADC and CBF reduction. These islands of small pixels will likely infarct but may not be identified as such based on ADC and/or CBF alone, thus affecting prediction accuracy. Noise in the data could also give rise to single pixels or small islands of normal ADC and/or CBF, resulting in reduced prediction accuracy. Second, incidence of ischemic injury includes distance from patent afferent vessels, basal regional blood flow, and metabolism. For example, the tissue close to the anterior communicating artery and the posterior cerebral artery has lower infarction incidence because of collateral flow (Shen *et al*, 2004*b*). Conversely, the hippocampus is thought to be more susceptible (Smith *et al*, 1984). Information regarding infarction incidence can be derived from an incident map of the infarct frequency, and can in principle be incorporated into the predictive model to improve prediction accuracy. Incorporation of these factors, however, may not be trivial because they may not be easily parameterized.

The artificial neural network (ANN), inspired by the neuronal networks in the central nervous system, is widely used in science and engineering for prediction and classification. It consists of nodes that are connected together to form a network with variable strengths (weights) between different connections. Through training, the relationship between inputs and outputs in the ANN can be mapped by altering the weights within the network. It is particularly useful in solving problems that have few obvious rules, problems that are difficult to specify mathematically, and problems that deal with a large number of parameters. ANN has been used for clustering of contrast-enhanced perfusion MRI data (Wismuller *et al*, 2006) and embolus detection using MRI (Kemeny *et al*, 1999). Prediction of functional outcome associated with clinical variables that are associated with rehabilitation in stroke (Oczkowski and Barreca, 1997) has also been described. Comparisons of ANN and other predictive models have also been reported (Tu, 1996).

The aim of this study was to develop and test a flexible predictive algorithm based on ANN to predict ischemic tissue fate using acute ADC and CBF data. Artificial neural network prediction algorithms were evaluated on rat stroke models subjected to three different occlusion durations (30-, 60-minute, and permanent MCAO). Predictions using ADC alone, CBF alone, and ADC + CBF were evaluated. In addition, the effects of neighboring pixels and infarction incidence on prediction accuracy were also evaluated. Prediction accuracy was quantified using receiver-operating characteristic (ROC) analysis. Comparisons of prediction accuracy were made with end-point T2-weighted MRI on a pixel-by-pixel basis.

Theory

The artificial neural network consists of interconnected nodes that form a network with variable weights between connections. Figure 1A shows the model of an artificial neuron. The relationship between the input and the output of the neuron can be described as

$$y = f\left(\sum_{i=1}^{n} w_i x_i + b\right), \tag{1}$$

where x_i is a input signal, w_i is the weight, y is the output, b is the threshold, and f is the activation function. A typical activation function and the one used here is the sigmoidal function:

$$f(t) = \frac{1}{1 + e^{-t}}. \tag{2}$$

Neural networks are formed by connecting these neurons together. This study used the feed-forward ANN, in which artificial neuron connections are arranged in layers in the direction from inputs to outputs without feedbacks among nodes in the same layer. Figure 1B shows the feed-forward ANN model with three layers, input layer, hidden layer, and output layer, in which the weights, bias, and other network connections were omitted for clarity. A supervised training of the ANN model was used. For the propagation of error, the back-propagation algorithm was used to minimize the cost function ξ on the output layer:

$$\xi = \frac{1}{2}\sum_{k=1}^{n} (y_k - Y_k)^2, \tag{3}$$

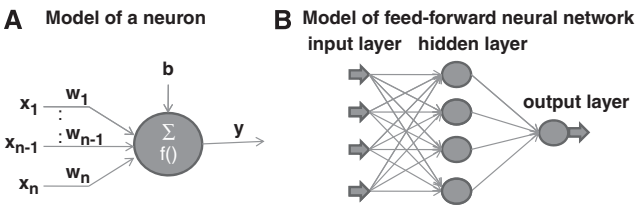

Figure 1 (**A**) A model of an artificial neuron and (**B**) a model of the feed-forward artificial neural network.

where y_k and Y_k are the actual and target outputs of the neuron k, and n is the number of neurons of the output layer. The essence of the back-propagation algorithm is to train the ANN algorithm by adjusting the weights of the network connections:

$$w_{ij}(t+1) = w_{ij}(t) + \Delta w_{ij}(t), \quad (4)$$

where w_{ij} is the weight between neuron i and neuron j. The training process was iterative and continued until the minimum training error, maximum training epochs, or minimum gradient of the error function was reached.

Instead of the commonly used gradient descent method to minimize cost function, this study used the resilient back-propagation method (Riedmiller and Braun, 1993) to speed up convergence. Resilient back propagation takes into account only the sign of the partial derivative over all patterns (not the magnitudes) and acts independently on each 'weight', as defined by

$$\Delta w_{ij}(t) = \begin{cases} -\Delta_{ij}(t), & \text{if } \frac{\partial \xi}{\partial w_{ij}}(t) > 0 \\ \Delta_{ij}(t), & \text{if } \frac{\partial \xi}{\partial w_{ij}}(t) < 0 \\ 0, & \text{else} \end{cases}, \quad (5)$$

where $\Delta_{ij}(t)$ is the update value corresponding to w_{ij} and is defined as

$$\Delta_{ij}(t) = \begin{cases} \eta^+ * \Delta_{ij}(t-1), & \text{if } \frac{\partial \xi}{\partial w_{ij}}(t-1) * \frac{\partial \xi}{\partial w_{ij}}(t) > 0 \\ \eta^- * \Delta_{ij}(t-1), & \text{if } \frac{\partial \xi}{\partial w_{ij}}(t-1) * \frac{\partial \xi}{\partial w_{ij}}(t) < 0 \\ \Delta_{ij}(t-1), & \text{else} \end{cases}, \quad (6)$$

with $0 < \eta^- < 1 < \eta^+$, Δ_0, $\Delta_{\max}$, and $\Delta_{\min}$ being the initial, maximum, and minimum values of Δ_{ij}, respectively. For each weight, if the partial derivative of the total error function compared with the last iteration changes sign, the update value for that weight is multiplied by η^-, where $\eta^- < 1$. If the last iteration yields the same sign, the update value is multiplied by η^+, where $\eta^+ > 1$. The update values are calculated for each weight and, in the end, each weight is replaced by its own update value, in the direction opposite to that weight's partial derivative. This approach is commonly used to accelerate convergence in a shallow region of the error function. Here, η^+ is empirically set to 1.2 and η^- to 0.5.

Materials and methods

Animal Preparations

The data used in this study were those of Shen and Duong (2008). In brief, a total of 36 Sprague–Dawley rats (300 to 350 g) were subjected to 30-minute ($n = 12$), 60-minute ($n = 12$), and permanent ($n = 12$) MCAO to enable comparison with a previously published prediction method (Shen and Duong, 2008). Stroke surgery and animal preparations have been described elsewhere (Meng *et al*, 2004; Shen *et al*, 2003, 2004*a*). A femoral artery was catheterized for blood-gas sampling, continuous blood pressure, and heart-rate monitoring. Blood pressure, heart rate, respiration rate, rectal temperature, and blood gases were maintained within normal physiologic ranges. Rats were initially anesthetized with chloral hydrate (400 mg/kg, intraperitoneally) and subjected to intraluminal MCAO. Once the animal was in the magnet, ~1% isoflurane was used. The animals breathed spontaneously without mechanical ventilation (Meng *et al*, 2004; Shen *et al*, 2005*a*). End-point T2-weighted MRI was performed at 24 hours after occlusion. Histological infarct volume was determined using TTC (2,3,5-triphenyltetrazolium chloride) staining and with edema correction (Meng *et al*, 2004).

Magnetic Resonance Experiments

Magnetic resonance imaging was performed on a Bruker 4.7-T/40-cm (Billerica, MA, USA) scanner. The animal was secured in a stereotaxic headset and placed onto an animal holder, consisting of a surface coil (2.3-cm inner diameter) for brain imaging and a butterfly neck coil for continuous arterial spin labeling (Meng *et al*, 2004). Coil-to-coil interaction was actively decoupled. Imaging was performed at 30, 60, 90, 120, and 180 minutes, and again at 24 hours after occlusion. For the 30- and 60-minute MCAO groups, the 30- and 60-minute data, respectively, were acquired before reperfusion. Reperfusion was accomplished remotely without taking the animal out of the scanner.

Quantitative CBF was measured using the continuous arterial spin-labeling technique (Duong *et al*, 2000) with gradient-echo echo-planar imaging (EPI), matrix = 128×128 (4 shots for the permanent MCAO group) or 64×64 (single shot for the 30- and 60-minute MCAO groups), field of view (FOV) = 2.56 cm × 2.56 cm, repetition time (TR) = 2 seconds per segment (90° flip angle), echo time (TE) = 20 milliseconds, and seven 1.5-mm slices. Paired images were acquired alternately—one with and the other without arterial spin-labeling preparation. In all, 76 pairs of images were acquired for signal averaging, with half acquired before and the other half after the ADC measurements.

The higher resolution in the permanent MCAO group was a result of our recent successful attempt to achieve better ischemic definition. Higher resolution could improve prediction by reducing the partial-volume effect, but it has lower signal-to-noise ratio (SNR) per unit time. Differences in resolution of the data here were not expected to alter the overall validity of the ANN approach.

Apparent diffusion coefficient maps were obtained by averaging three data sets acquired with diffusion-sensitive gradients applied along the x, y, or z direction, using spin-echo EPI, matrix = 128×128 (4 shots for the permanent MCAO group) or 64×64 (single shot for the 30- and 60-minute MCAO groups), FOV = 2.56 cm × 2.56 cm, TR = 2 seconds per segment (90° flip angle), TE = 37.5 milliseconds, seven 1.5-mm slices, and 16 averages, $b = 10$, and three directions of 1,270 s/mm^2, $\Delta = 17.53$ ms, and $\delta = 5.6$ ms.

At 24 hours after occlusion, T2-weighted images were acquired using the fast spin-echo pulse sequence (echo time per echo = 6.5 milliseconds) with two different effective echo times (52 and 104 milliseconds), echo train length 16, and 16 signal averages.

Data Analysis

Five anterior slices were analyzed to avoid susceptibility distortion around the ear canals. Images were coregistered using custom-designed semiautomatic coregistration software between acute-phase and 24-hour data within the same animals and between animals as described previously (Liu *et al*, 2004; Schmidt *et al*, 2006; Shen *et al*, 2005*a*). Apparent diffusion coefficient maps with intensity in units of mm^2/s (Meng *et al*, 2004; Shen *et al*, 2005*a*) and CBF maps with intensity in units of mL per gram per min were calculated (Duong *et al*, 2000) as described previously using codes written in Matlab (MathWorks, Natick, MA, USA). Image displays and overlays were performed using the STIMULATE software (University of Minnesota). All data were reported as mean ± s.e.m.

Cluster Analysis: The iterative self-organizing data analysis algorithm (ISODATA; Ball and Hall, 1965) was used to segment and exclude pixels of the cerebrospinal fluid and the corpus callosum (Shen *et al*, 2004*b*). With the remaining gray matter in the rat brain, ISODATA was then used to identify pixels belonging to different tissue zones based on ADC and CBF data, and to determine the final lesion volume based on end-point MRI data. Multiple clusters were resolved and identified as 'normal', 'mismatch,' and 'ischemic core' from the ischemic right hemisphere at each acute time point (Shen *et al*, 2004*b*). The final lesion was determined using ADC and T2 maps at 24 hours after occlusion.

Spatial Infarction Incidence: To improve prediction accuracy, spatial infarction incidence maps were obtained by counting the frequency of infarction for each MCAO group (which is known as the spatial frequency of infarct; Shen *et al*, 2005*b*). Images from different animals within the same MCAO group were spatially coregistered and the infarction incidence maps were computed pixel by pixel using,

$$\text{Spatial infarction incidence}\,(x, y, z) = \frac{\text{number of animals in which pixel}\,(x, y, z)\,\text{was infarcted}}{\text{number of total animals}}$$

where x ranged from 1 to 64 or 128, y ranged from 1 to 64 or 128, and z ranged from 1 to 4 (number of slices). Note that spatial continuity was not used in our analysis.

Artificial Neural Network: Artificial neural network algorithms were developed in the Matlab environment using the ANN toolbox. Three experimental groups were analyzed: permanent, 60-, and 30-minute MCAO groups. The ANN was trained and tested using the leave-one-out method—i.e., one animal was used as the 'test' subject and the remaining animals in the same MCAO group were used as 'training' subjects. This was cycled for all animals in the same group.

The number of hidden neurons and the number of training epochs were optimized for ADC alone. The number of hidden neurons was evaluated from 1, 2, 4, 6, 8, 10, 12, 14, 16, 18, and 20 (with the number of training epochs being 150). The number of training epochs was evaluated from 5, 10, 15, 20, 25, and 50, and from 100 to 500 in steps of 100 (with the number of hidden neurons being 5). The optimal number of training epochs and the number of hidden neurons were those that yielded the largest areas under the ROC curves.

Artificial neural network predictions were made for the 30-, 60-minute and permanent MCAO groups using their corresponding ANN basis sets, namely: (1) the permanent MCAO ANN basis set was trained and applied to permanent MCAO animals for prediction, (2) the 60-minute MCAO ANN basis set was trained and applied to the 60-minute MCAO animals for prediction, and (3) the 30-minute MCAO ANN basis set was trained and applied to the 30-minute MCAO animals for prediction. For each MCAO data set, training was performed for six conditions: (1) CBF alone, (2) ADC alone, (3) ADC + CBF, (4) ADC + CBF + two-dimensional (2D) adjacent pixels, (5) ADC + CBF + 3D adjacent pixels, and (6) ADC + CBF + 3D adjacent pixels + spatial information. For each MCAO data set, predictions were then made using only data obtained at 30 minutes after stroke onset for each of the six conditions. Adjacent pixels referred to 8 and 26 immediate neighbor pixels in 2D and 3D, respectively, in which they were treated as independent inputs of ANN. For example, there were 18 inputs for the ADC + CBF + 2D condition (i.e., for each ADC pixel there were eight neighbors, totaling nine inputs, and for each CBF pixels there were eight neighbors, totaling nine inputs). Spatial information referred to the infarction incidence map described above.

To further evaluate the hypothetical treatment effects, prediction was also made for the permanent, 60-, and 30-minute MCAO groups using only the permanent MCAO ANN training basis set. Predictions were made for the six conditions described above.

For ANN analysis, the initial value of all update values Δ_{ij} was set as 0.01 (equation (6)). To prevent the weights from becoming too large, the maximum weight step determined by the size of the update value was limited, with the upper bound being arbitrarily set as $\Delta_{max} = 50$. The minimum step size was fixed at $\Delta_{min} = 1e^{-6}$.

Receiver-operating characteristic analysis was performed to evaluate the prediction accuracy as described previously (Shen *et al*, 2005*b*). Sensitivity and specificity at the optimal point and the areas under the ROC curves (AUCs) were tabulated for comparison.

Comparison With a Previously Published Prediction Model

Comparison of prediction performance (AUC) by ANN was also made using a previously published probabilistic prediction model, using the identical data sets as described in Shen *et al* (2005*b*) and Shen and Duong (2008).

Statistical Analysis

Two-way analysis of variance (ANOVA) with multiple-comparisons Tukey–Kramer's correction was used for comparison among different conditions (Figures 5 and 6). The paired *t*-test was used for comparison between prediction made when training with its own basis set and that made when training with the permanent MCAO basis set (Figure 7).

Results

Spatial infarction incidence maps were derived (Figure 2). Spatial infarction incidence and the extent of infarction were heterogeneous. The ischemic core has a comparatively high infarction incidence as expected, whereas the mismatch region has a nonzero infarction incidence and the normal tissue has close to zero infarction incidence. The spatial infarction incidence varied significantly across the three experimental stroke groups.

Figure 3 shows the optimization of the number of hidden neurons and the number of training epochs for the ADC data obtained from the permanent, 60-, and 30-minute MCAO groups. The optimal AUC reached a plateau at 6 hidden neurons and 40 training epochs for all MCAO groups for ADC data alone. On the basis of these optimization results, we performed additional optimizations using 7 hidden neurons and 50 training epochs for all other conditions (ADC, CBF, ADC + CBF, ADC + CBF + 2D, ADC + CBF + 3D, and ADC + CBF + 3D + spatial information). The AUCs were not statistically different from the plateau values shown in Figure 3 for all conditions. Thus, it was sufficient in all subsequent analysis of ANN trainings with 7 hidden neurons and 50 training epochs for all conditions.

Representative data sets of the pixel-by-pixel ANN predictions of subsequent infarction are shown in Figure 4 for the three experimental stroke groups under various conditions. Predictions for each MCAO group used its own basis set and MRI data obtained at 30 minutes after ischemia. The conditions evaluated were CBF alone, ADC alone, ADC + CBF, ADC + CBF + 2D, ADC + CBF + 3D, and ADC + CBF + 3D + spatial information. For references, ADC, CBF maps, and ISODATA analysis of lesion volume based on ADC and T2 are also shown. ISODATA analysis of lesion volume (shown as blue pixels) was taken as the end-point measure, which had been previously correlated with histology (Shen *et al*, 2005*b*; Shen and Duong, 2008).

The major findings from Figure 4 are as follows. For the permanent MCAO group, the predicted infarct maps showed generally good pixel-by-pixel correspondence with ISODATA cluster analysis of the end-point MRI data, with the exception of CBF data alone, which poorly predicted the infarct. With additional information (going from top to bottom), predictions were slightly more accurate regarding lesion location and volume, as well as slightly more certain (i.e., stronger yellow pixels). For the 60- and 30-minute MCAO groups, prediction with CBF alone was inaccurate and less certain (stronger orange pixels) compared with the permanent MCAO group. With additional information (going from top to bottom), predictions were more accurate and more certain. Predicted maps are in general agreement with ISODATA analysis of lesion volume.

Quantitative analyses of group data are summarized below. Figure 5 shows the AUCs for predictions

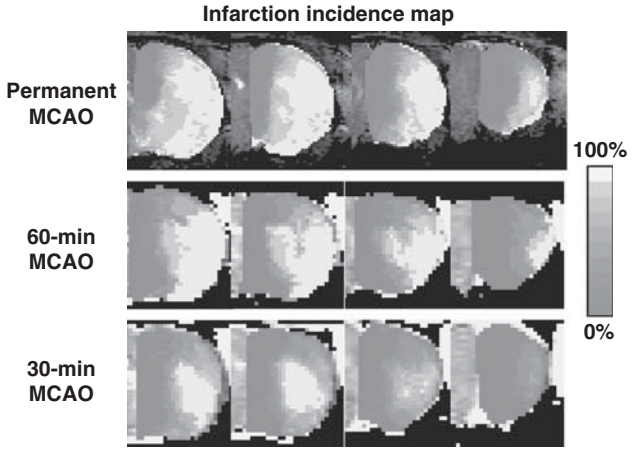

Figure 2 Spatial infarction incidence maps for the permanent, 60-, and 30-minute middle cerebral artery occlusion (MCAO) groups. The color bar denotes the infarction incidence from 0% to 100%. The color reproduction of this figure is available on the html full text version of the manuscript.

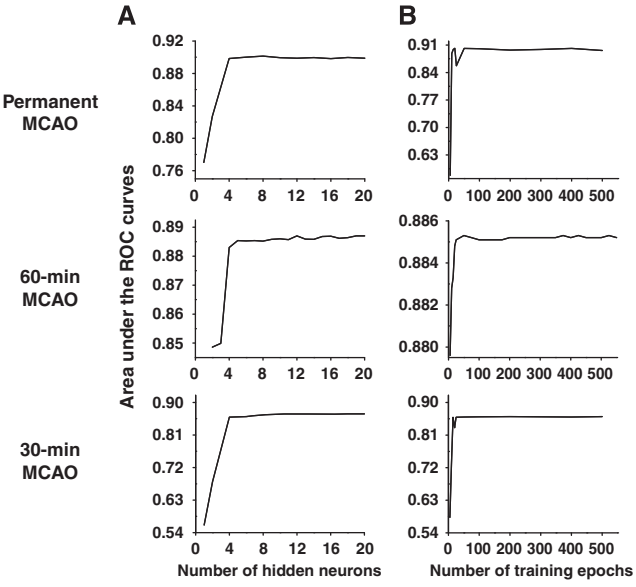

Figure 3 Optimization of (**A**) the number of hidden neurons and (**B**) the number of training epochs for apparent diffusion coefficient (ADC) data obtained from the permanent middle cerebral artery occlusion (MCAO), 60-minute MCAO, and 30-minute MCAO groups.

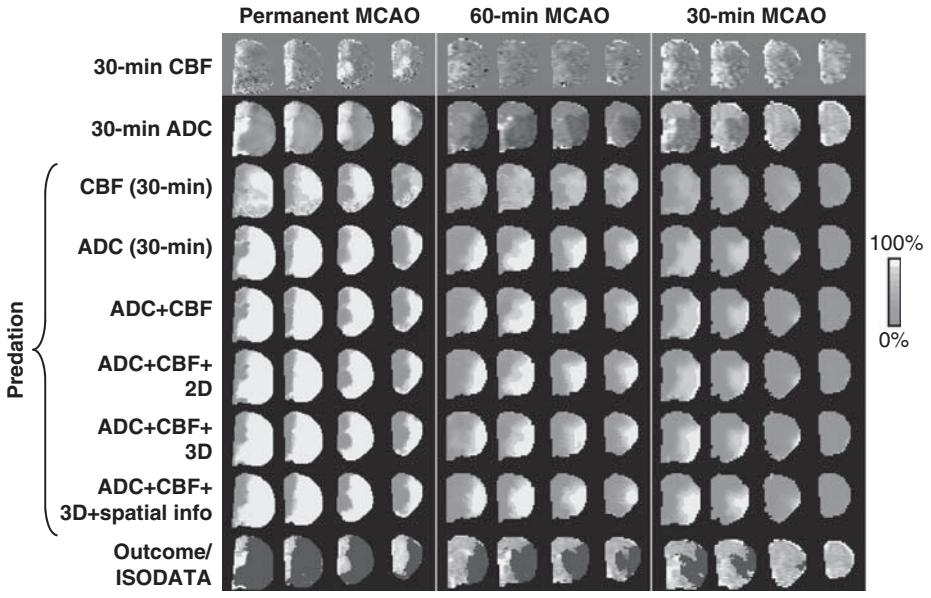

Figure 4 Predicted infarct maps for the permanent, and 60-, and 30-minute middle cerebral artery occlusion (MCAO) groups using their own artificial neural network (ANN) training basis sets. Multislice images are posterior to the anterior slices from left to right. Predictions were made with cerebral blood flow (CBF) alone, apparent diffusion coefficient (ADC) alone, ADC + CBF, ADC + CBF + 2D adjacent pixels, ADC + CBF + 3D adjacent pixels, and ADC + CBF + 3D adjacent pixels + spatial information. For references, ADC, CBF maps, and iterative self-organizing data analysis algorithm (ISODATA) analysis of end-point lesion volume based on ADC and T2 are also shown. Color bar denotes the probability of infarct from 0% to 100%. The color reproduction of this figure is available on the html full text version of the manuscript.

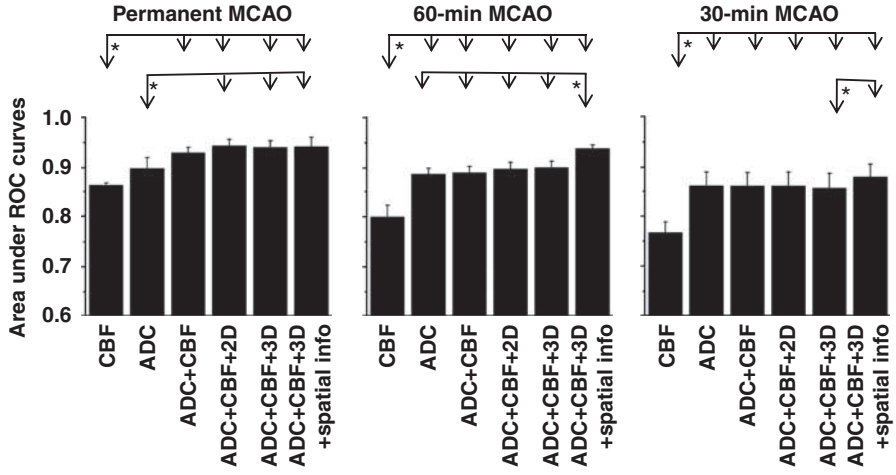

Figure 5 The areas under receiver-operating characteristic (ROC) curves for the three different occlusion durations: permanent, 30- and 60-minute middle cerebral artery occlusion (MCAO). Predictions for each MCAO group training with its own basis set. Two-way analysis of variance (ANOVA) with multiple comparisons applying Tukey–Kramer's correction; $*P < 0.05$.

of each MCAO group using its own training basis set. The general observations were the following: (1) CBF alone at 30 minutes poorly predicted infarct across all three experimental groups; (2) ADC alone adequately predicted infarct; (3) CBF + ADC improved the prediction accuracy; (4) addition of neighboring pixel information in 2D and 3D only slightly improved prediction accuracy; (5) addition of infarction incidence further improved prediction accuracy slightly; and (6) finally, prediction was more accurate for the permanent MCAO group, followed by the 60- and 30-minute MCAO groups.

Specifically, within each MCAO group, predictions made using CBF alone were significantly different from those obtained using other conditions (i.e., ADC + CBF, ADC + CBF + 2D, ADC + CBF + 3D, and ADC + CBF + 3D + spatial information). Furthermore, in the 60-minute MCAO group, the ADC + CBF + 3D + infarction incidence condition showed more significant difference than all other conditions

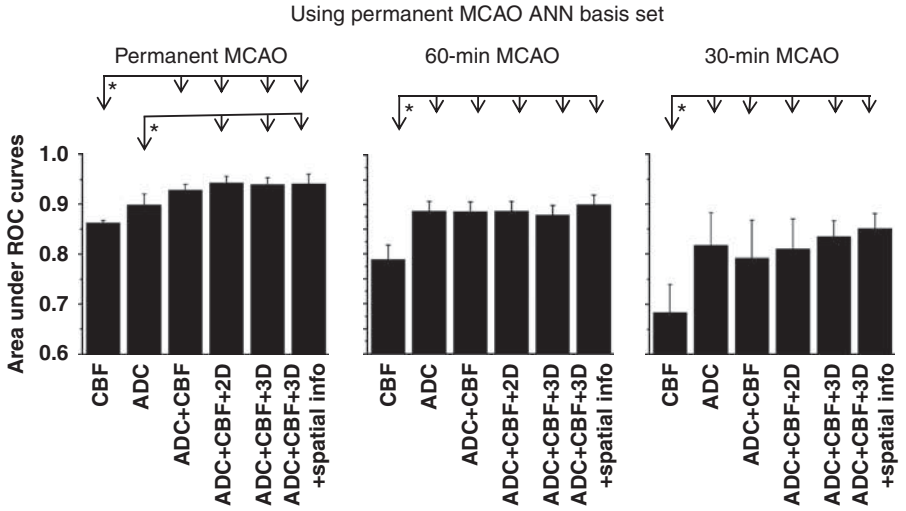

Figure 6 The areas under receiver-operating characteristic (ROC) curves for the three different occlusion durations: permanent, 30- and 60-minute middle cerebral artery occlusion (MCAO). Predictions for all MCAO groups training with the *permanent* MCAO basis set. The panel for the permanent MCAO group is identical to that shown in Figure 5.

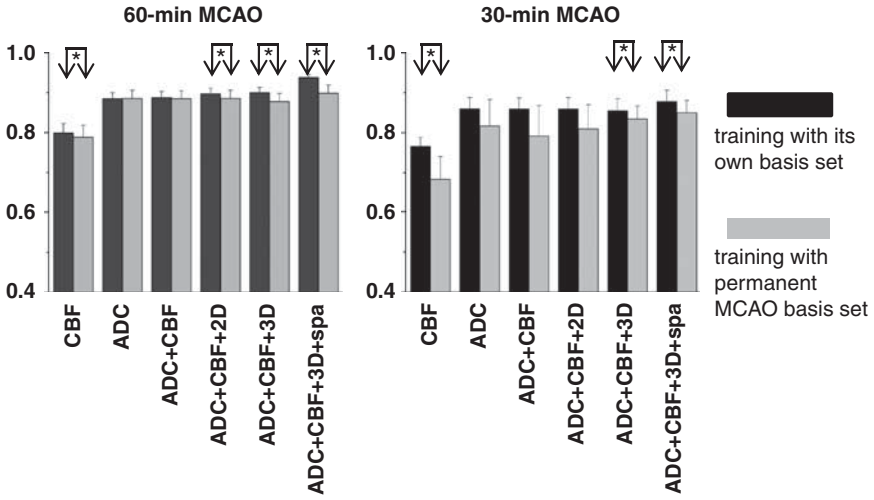

Figure 7 Statistical comparison between prediction made with training with its own basis set and that made with the permanent middle cerebral artery occlusion (MCAO) basis set. This figure is a re-plot of Figures 5 and 6 to allow side-by-side comparison. $^*P < 0.05$ (paired *t*-test).

($P < 0.05$, two-way ANOVA with multiple-comparisons Tukey–Kramer's correction).

To evaluate the effects of reperfusion, predictions for the 30- and 60-minute MCAO groups were made using the *permanent* MCAO training basis set (Figure 6). Areas under the curve for the 30- and 60-minute MCAO predictions using the permanent MCAO basis set (Figure 6) were smaller than those obtained using their corresponding basis sets (Figure 5). The statistical paired *t*-test comparisons are shown in Figure 7.

Comparison With a Previously Published Prediction Model

The AUCs of prediction performance using a previously published probabilistic prediction model (Shen *et al*, 2005*b*; Shen and Duong, 2008) are summarized in Table 1. There were no statistical differences between prediction performances (AUCs) obtained using ANN in this study and those obtained by Shen *et al* (2005*b*) and Shen and Duong (2008).

Discussion

A flexible ANN algorithm was developed to predict the ischemic tissue fate pixel by pixel based on multimodal MRI data of acute stroke. The efficacy of the ANN prediction algorithm was evaluated using reproducible rodent stroke models of various occlusion durations. Predictions showed the likelihood of future infarction on a pixel-by-pixel

Table 1 Comparison of AUC from the probabilistic prediction algorithm (Shen *et al*, 2005*b*; Shen and Duong, 2008) and the corresponding AUC from ANN

	ADC+CBF	*ADC+CBF+ spatial*	*ADC+CBF+ 3D+spatial*
Permanent MCAO			
Probabilistic	93 ± 3	92 ± 4	NA
ANN	93 ± 1	95 ± 4	94 ± 2
60-minute MCAO			
Probabilistic	90 ± 4	92 ± 3	NA
ANN	89 ± 2	94 ± 1	94 ± 1
30-minute MCAO			
Probabilistic	87 ± 3	92 ± 3	NA
ANN	86 ± 3	89 ± 3	88 ± 3

ADC, apparent diffusion coefficient; ANN, artificial neural network; AUC, area under the curve; CBF, cerebral blood flow; 3D, three-dimensional; Spatial, spatial information; MCAO, middle cerebral artery occlusion; NA, not analyzed.

basis. Moreover, accounting for neighboring pixels and infarction incidence improved the prediction accuracy. These results could have important clinical applications.

Artificial Neural Network Algorithms

A key advantage of the ANN prediction algorithm is that it does not need the exact mathematical relation between input and output parameters. A case in point is that incorporation of the spatial information does not require it to be explicitly parameterized. Another advantage of the ANN prediction algorithm is that the training sample sizes can be augmented readily as more data sets become available. The number of image and other input parameters can be large. A disadvantage of the ANN prediction algorithm is that the computational time increases very rapidly with the number of parameters (neurons or layers). However, this is only a one-time computational cost that is incurred during 'training' of the ANN.

Determining the optimal numbers of hidden nodes and training epochs remains a major unsolved problem in ANN. The majority of the studies used an arbitrary number of hidden nodes and training epochs (Jorjani *et al*, 2008; Landeras *et al*, 2008; Zhang *et al*, 2008). In this study, we explicitly optimized the number of hidden nodes and number of training epochs. From these data, we found rapid convergence for the AUCs. The AUC reached a plateau at 6 hidden neurons and 40 training epochs for all MCAO groups.

Accounting for Neighboring Pixels

In the ANN prediction algorithms, neighboring pixels were treated as independent inputs, which is not the same as (but may have a similar effect as) spatial smoothing. Accounting for neighboring pixels generally improved the prediction performance, although doing so did not yield statistically significant difference. By inclusion of the nearest-neighborhood information, the 'noise' effect from 'single pixel' errors on prediction could be minimized. However, inclusion beyond the nearest neighbors would likely improve AUC but could also potentially obscure identification of interesting heterogeneous areas, such as the ischemic penumbra. In this study, only the immediate neighboring pixels (8 neighbors in 2D and 26 neighbors in 3D) were used.

Comparison Among Predictive Models

Using the voxel-based generalized linear model algorithm, Wu *et al* (2007) predicted infarction in normal and hypertensive stroke rats that were subjected to embolic clot occlusion with and without recombinant tissue plasminogen activator (rt-PA) treatment at 1 hour after stroke. They found that pretreatment-predicted outcome compared with posttreatment histology was highly accurate in saline-treated rats (92% ± 5%). Accuracy was significantly reduced in rt-PA-treated animals (86% ± 8%). Animals that reperfused had significantly lower GLM-predicted infarction risk than nonreperfused animals, suggesting that tissue was more amenable to therapy. In another study, Wu *et al* (2001) compared the GLM prediction and thresholding methods applied on human stroke data. At their optimal operating points, thresholding algorithms combining DWI and PWI provided 66% sensitivity and 83% specificity, and GLM algorithms combining DWI and PWI predicted with 66% sensitivity and 84% specificity voxels that proceeded to infarct. Thresholding algorithms that combined DWI and PWI provided significant improvement to algorithms that used DWI alone but showed no significant improvement over algorithms that used PWI alone. GLM algorithms that combined DWI and PWI showed significant improvement over algorithms that used only DWI or PWI. The performances of thresholding and GLM algorithms were found to be comparable.

Shen *et al* (2005*b*) and Shen and Duong (2008) documented the probability-of-infarct profiles of stroke rats that underwent different MCAO durations. Using only acute ADC and CBF data, pixel-by-pixel prediction was made and compared with end-point T2 imaging and histology. The ANN method showed slightly better performance. However, there were no statistical differences between the prediction performance (AUCs) of ANN obtained in this study and that obtained by Shen *et al* (2005*b*) and Shen and Duong (2008). Although there were some minor methodological differences in the assignment of training groups, this comparison indicates that the two approaches yielded comparable performance. The key advantage of ANN is that ANN offers flexibility and can be readily extended to a large number of input parameters.

In this study using ANN prediction algorithms, the areas under the ROC were 86% ± 3%, 89% ± 2%, and 93% ± 1% using ADC + CBF for the 30-, and 60-minute, and permanent MCAO, respectively. We further reported that adding neighboring pixel information and spatial information markedly improved performance measures over ADC and CBF alone for the 60- and 30-minute MCAO group (88% ± 3% and 94% ± 1%, respectively), but only slightly for the permanent MCAO group (94% ± 2%). These differences were expected because permanent MCAO was less variable and could be sufficiently and accurately accounted for with ADC and CBF. Moreover, to determine the hypothetical effects of reperfusion on prediction, predictions for the 30- and 60-minute MCAO groups were also done by using the *permanent* MCAO basis set. Areas under the curve for the 30- and 60-minute MCAO predictions using the *permanent* MCAO basis set were smaller than those for the permanent MCAO prediction, suggesting that tissue was likely more amenable to therapy.

In short, these quantitative prediction models (GLM; Wu *et al*, 2007), probabilistic model (Shen *et al*, 2005*b*; Shen and Duong, 2008), and ANN (this study)) based on acute ADC and CBF data were accurate and yielded comparable AUCs on animal stroke models. Differences in animal stroke models (embolic versus suture), anesthetics (halothane versus isoflurane), and inclusion of slightly different types of MRI data (dynamic susceptibility contrast versus arterial spin labeling of CBF) prevented quantitative comparison. Accounting for infarction incidence improved the prediction accuracy. These predictive algorithms have the potential to serve as promising metrics for diagnosis, prognosis, and therapeutic evaluation of acute stroke.

Future Perspective

Prediction of tissue fate was reasonably accurate despite the small sample sizes in this study. Human stroke is more heterogeneous and so prediction is likely to be less accurate. The major challenge for predictive modeling in stroke is categorization of the type of stroke (i.e., permanent and transient ischemia) *a priori*. In a clinical setting, establishing proper training basis sets and selecting the proper algorithms to apply is expected to be challenging because human stroke is more heterogeneous and the stroke onset time is not well defined. Future studies will attempt to use 'model selection' to determine which basis set should be applied to a specific stroke subject. Prediction of human stroke requires segmentation of gray and white matters (white matter was segmented out in this study and was ignored because of its small volume; Shen *et al*, 2005*b*) because they have different susceptibilities to infarction. Incorporation of additional information such as functional MRI (Dijkhuizen *et al*, 2003; Shen *et al*, 2005*a*), vascular permeability (Dijkhuizen *et al*, 2002), oxygen consumption, oxygen extraction fraction (An and Lin, 2000), metabolic profile, and/or relaxation time measurements in stroke is expected to improve the prediction accuracy. These parameters can be readily incorporated in this ANN approach.

The ANN prediction model may also be applied to other imaging data such as those obtained from transient ischemic attack. Many patients with transient ischemic attack often return to the emergency room with large stroke within 48 hours (Rothwell and Warlow, 2005). Translating the success of basic therapeutic research into proven interventions in humans has been challenging. Objective and accurate prediction models of tissue fate may provide a framework in clinical decision making and may help drug trials by accelerating the identification of the promising potential therapies. Finally, this predictive approach could individualize the treatment window for stroke patients and extend current treatment window options.

Conclusions

This study establishes a flexible ANN predictive algorithm model and incorporates neighboring pixel and infarction incidence information to improve the prediction accuracy of ischemic tissue fate. The ANN prediction model has potential clinical applications towards providing quantitative and objective frameworks to aid clinical decision making in the treatment of acute stroke, testing therapeutic treatments, and tailoring individual treatment.

Conflict of interest

The authors declare no conflict of interest.

References

An H, Lin W (2000) Quantitative measurements of cerebral blood oxygen saturation using magnetic resonance imaging. *J Cereb Blood Flow Metab* 20:1225–36

Arenillas JF, Rovira A, Molina CA, Grive E, Montaner J, Alvarez-Sabin J (2002) Prediction of early neurological deterioration using diffusion- and perfusion-weighted imaging in hyperacute middle cerebral artery ischemic stroke. *Stroke* 33:2197–203

Astrup J, Sorensen PM, Sorensen HR (1981*a*) Oxygen and glucose consumption related to Na+/K+ transport in canine brain. *Stroke* 12:726–30

Astrup J, Symon L, Siesjo BK (1981*b*) Thresholds in cerebral ischemia: the ischemic penumbra. *Stroke* 12:723–5

Ball GH, Hall DJ (1965) *ISODATA: a novel method of data analysis and pattern classification*, Vol. 4. Menlo Park, CA: Stanford Research Institute, 1–60

Dijkhuizen RM, Asahi M, Wu O, Rosen BR, Lo EH (2002) Rapid breakdown of microvascular barriers and subsequent hemorrhagic transformation after delayed recombinant tissue plasminogen activator treatment in a rat embolic. *Stroke* 33:2100–4

Dijkhuizen RM, Singhal AB, Mandeville JB, Wu O, Halpern EF, Finklestein SP, Rosen BR, Lo EH (2003) Correlation between brain reorganization, ischemic damage, and neurologic status after transient focal cerebral ischemia in rats: a functional magnetic resonance imaging study. *J Neurosci* 23:510–7

Duong TQ, Silva AC, Lee S-P, Kim S-G (2000) Functional MRI of calcium-dependent synaptic activity: cross correlation with CBF and BOLD measurements. *Magn Reson Med* 43:383–92

Guadagno JV, Warburton EA, Jones PS, Fryer TD, Day DJ, Gillard JH, Carpenter TA, Aigbirhio FI, Price CJ, Baron JC (2005) The diffusion-weighted lesion in acute stroke: heterogeneous patterns of flow/metabolism uncoupling asassessed by quantitative positron emission tomography. *Cerebrovasc Dis* 19:239–46

Hossmann K-A (1994) Viability thresholds and the penumbra of focal ischemia. *Ann Neurol* 36:557–65

Jorjani E, Chehreh Chelgani S, Mesroghli SH (2008) Application of artificial neural networks to predict chemical desulfurization of Tabas coal. *Fuel* 87:2727–34

Kemeny V, Droste DW, Hermes S, Nabavi DG, Schulte-Altedorneburg G, Siebler M, Ringelstein EB (1999) Automatic embolus detection by a neural network. *Stroke* 30:807–10

Kidwell CS, Alger JR, Saver JL (2003) Beyond mismatch: evolving paradigms in imaging the ischemic penumbra with multimodal magnetic resonance imaging. *Stroke* 34:2729–35

Landeras G, Ortiz-Barredo A, Lopez J (2008) Comparison of artificial neural network models and empirical and semi-empirical equations for daily reference evapotranspiration estimation in the Basque Country (Northern Spain). *Agric Water Manage* 95:553–65

Liu ZM, Schmidt KF, Sicard KM, Duong TQ (2004) Imaging oxygen consumption in forepaw somatosensory stimulation in rats under isoflurane anesthesia. *Magn Reson Med* 52:277–85

Lo EH, Moskowitz MA, Jacobs TP (2005) Exciting, radical suicidal: how brain cell die after stroke. *Stroke* 36:189–92

Meng X, Fisher M, Shen Q, Sotak CH, Duong TQ (2004) Characterizing the diffusion/perfusion mismatch in experimental focal cerebral ischemia. *Ann Neurol* 55:207–12

Oczkowski WJ, Barreca S (1997) Neural network modeling accurately predicts the functional outcome of stroke survivors with moderate disabilities. *Arch Phys Med Rehabil* 78:340–5

Riedmiller M, Braun H (1993) A direct adaptive method for faster backpropagation learning: the RPROP algorithm. In: *Proceedings of the IEEE International Conference on Neural Networks (ICNN)* (Ruspini H, ed), San Francisco, USA

Rothwell PM, Warlow CP (2005) Timing of transient ischemic attacks preceding ischemic stroke. *Neurology* 64:817–20

Schmidt KF, Febo M, Shen Q, Ferris CF, Stein E, Duong TQ (2006) Hemodynamic and metabolic changes induced by cocaine in anesthetized rat observed with multimodal functional. *Psychopharmacology* 185:479–86

Shen Q, Duong TQ (2008) Quantitative prediction of ischemic stroke tissue fate. *NMR Biomed* 21:839–48

Shen Q, Fisher M, Sotak CH, Duong TQ (2004*a*) Effects of reperfusion on ADC and CBF pixel-by-pixel dynamics in stroke: characterizing tissue fates using quantitative diffusion and perfusion imaging. *J Cereb Blood Flow Metab* 24:280–90

Shen Q, Meng X, Fisher M, Sotak CH, Duong TQ (2003) Pixel-by-pixel spatiotemporal progression of focal ischemia derived using quantitative perfusion and diffusion imaging. *J Cereb Blood Flow Metab* 23:1479–88

Shen Q, Ren H, Bouley J, Fisher M, Duong TQ (2004*b*) Dynamic tracking of acute ischemic tissue fates using improved unsupervised ISODATA analysis of high-resolution quantitative perfusion and diffusion data. *J Cereb Blood Flow Metab* 24:887–97

Shen Q, Ren H, Cheng H, Fisher M, Duong TQ (2005*a*) Functional, perfusion and diffusion MRI of acute focal ischemic brain injury. *J Cereb Blood Flow Metab* 25:1265–79

Shen Q, Ren H, Fisher M, Duong TQ (2005*b*) Statistical prediction of tissue fates in acute ischemic brain injury. *J Cereb Blood Flow Metab* 25:1336–45

Smith M-L, Auer RN, Siesjö BK (1984) The density and distribution of ischemic brain injury in the rat following 2–10 min of forebrain ischemia. *Acta Neuropathol* 64:319–32

Sobesky J, Zaro Weber O, Lehnhardt FG, Hesselmann V, Neveling M, Jacobs A, Heiss WD (2005) Does the mismatch match the penumbra? Magnetic resonance imaging and positron emission tomography in early ischemic stroke. *Stroke* 36:980–5

Thomalla GJ, Kucinski T, Schoder V, Fiehler J, Knab R, Zeumer H, Weiller C, Rother J (2003) Prediction of malignant middle cerebral artery infarction by early perfusion- and diffusion-weighted magnetic resonance imaging. *Stroke* 34:1892–900

Tu JV (1996) Advantages and disadvantages of using artificial neural networks versus logistic regression for predicting medical outcomes. *J Clin Epidemiol* 49:1225–31

Warach S (2003) Measurement of the ischemic penumbra with MRI: it's about time. *Stroke* 34:2533–4

Wismuller A, Meyer-Baese A, Lange O, Reiser MF, Leinsinger G (2006) Cluster analysis of dynamic cerebral contrast-enhanced perfusion MRI time-series. *IEEE Trans Med Imaging* 25:62–73

Wu O, Koroshetz WJ, Ostergard L, Buonanno FS, Copen W, Gonzales RG, Rordorf G, Rosen BR, Schwamm LH, Weisskoff RM, Sorensen AG (2001) Predicting tissue outcome in acute human cerebral ischemia using combined diffusion-and perfusion-weighted MR imaging. *Stroke* 32:933–42

Wu O, Sumii T, Asahi M, Sasamata M, Ostergaard L, Rosen BR, Lo EH, Dijkhuizen RM (2007) Infarct prediction and treatment assessment with MRI-based algorithms in experimental stroke models. *J Cereb Blood Flow Metab* 27:196–204

Zhang L, Wu K, Zhong Y, Li P (2008) A new sub-pixel mapping algorithm based on a BP neural network with an observation model. *Neurocomputing* 71:2046–54